Peripheral collisions of highly charged ions with metal clusters*

Zhang Cheng-Jun(张成俊), Hu Bi-Tao(胡碧涛)†, and Luo Xian-Wen(罗先文)

School of Nuclear Science and Technology, Lanzhou University, Lanzhou 730000, China

(Received 2 September 2011; revised manuscript received 16 November 2011)

Within the framework of the dynamical classical over-barrier model, the soft collisions between slow highly charged ions (SHCIs) Ar^{17+} and the large copper clusters under large impact parameters have been studied in this paper. We present the dominant mechanism of the electron transfer between SHCIs and a large metal cluster by computational simulation. The evolution of the occupation of projectile ions, KL^x satellite lines, X-ray yields, Auger electron spectrum and scattering angles are provided.

Keywords: highly charged ion, metal cluster, collision

PACS: 36.40.Wa, 32.30.Rj, 34.70.+e, 61.46.–w **DOI:** 10.1088/1674-1056/21/5/053601

1. Introduction

Within the past few years, the interaction between SHCIs and various targets such as atoms, molecules, clusters, bulk metals, and insulating surfaces has been studied extensively and rapidly in experiments and theories.[1,2] Especially, cluster targets have received a great deal of attention due to their intermediate structures between atoms and solids, and their natural exotic properties.[3] A cluster target presents both atom and bulk target characteristics. Similar to the solid, it has a large number of electrons with nearly the same energy levels and allows multiple electronic transition. It is also similar to the ion-atom case in which the interaction time is limited. In addition, a "hollow ion" will be formed during the impact process and survive until becoming de-excited on its leaving path. Several groups have tried to find the connection between the understanding of ion-atom and ion-surface collisions[4−13] in the past few years. It has been observed that the collisions between SHCIs and atomic clusters could produce multiple charged clusters. In the peripheral collision, removing electrons from the cluster by using SHCIs is a very gentle process and the energy transferred to the cluster is relatively small, so it is possible to create fairly cool cluster ions[14] with highly charged states.

The basic main physical processes of the ion-matter interaction are transfer of electrons between the target and the projectile ion, final charge state distribution, electron emission, and X-ray emission. Several theoretical models were used to deal with these different cases, in which the most common and brief model is the classical over-barrier model. This model[15] and its variants[16,17] have provided the main features of the charge transfer in ion-atom[2,15,18] and ion-surface[17,19] collisions successfully. The first investigation of the interaction between the highly charged ion and the cluster was performed by Watch *et al.*[4] for 80-keV Ar^{8+} + C_{60} collisions where they obtained stable C_{60}^{s+} ions with s ranging up to 6, which proved directly that peripheral colliding with SHCI is an efficient way to produce stably and multiply charged cluster ions. Two years later, Jin *et al.*[20] observed intact C_{60}^{9+} produced by slow Bi^{44+}. Even the charge state reached 10 by Xe^{25+} impacting in Huber's work.[21]

From a theoretical point of view, Thumm[22] firstly extended a dynamic classical over-barrier model into ion-C_{60} interaction, and used it to calculate translational energy gain,[23] which was mainly in good agreement with the result measured by Selberg *et al.*[24] There are many other theoretic works, however, most of them focus on the fullerenes. Plagne and Guet *et al.*[25,26] have studied the peripheral collision between Xe^{25+} and a neutral alkali-metal Na_{196} cluster. They used the semi-classical approximations of targets and calculated the dynamical response of the delocalized valence electrons as the highly charge

*Project supported by the National Natural Science Foundation of China (Grant Nos. 11135002, 91026021, 11075068, 11075069, and 10975065) and the Fundamental Research Funds for the Central Universities of China (Grant No. lzujbky-2010-k08).

†Corresponding author. E-mail: hubt@lzu.edu.cn

© 2012 Chinese Physical Society and IOP Publishing Ltd

ions passed by, and got reasonable results, especially for the excitation energy. However, there were some limits, for instance, hollow atom formation, decay during the collision and that the detail of charge transfer were not considered.

In this paper, we try to extend the dynamical classical over-barrier model and discuss theoretical predictions of the electron response in ion–metal cluster collisions, present the detailed evolution of hollow-ions and the effect of collision parameters on the charge state, level occupations, inner shell X-ray emission and scattering angles. The organization of this paper is as following. In Section 2, we give a detailed description of the simulation model, including the ion motion, the mechanism of the electron transfer, the inner shell decay, and the X-ray emission. The calculation results are be discussed in Section 3. At the end, a short conclusion is presented.

2. Model and method

Assuming that a cluster is an infinitely conducting sphere without resistance. When a highly charged ion approaches the sphere, the conductive electrons will be attracted by the ion, and an inhomogeneous charge distribution will be built up on the surface of the cluster. The electric field in the cluster sphere is zero but the field out of the cluster sphere is determined by the electrostatic images[28] of the projectile ion and the active electrons.

We attempt to interpret the whole electron-transfer process in terms of the over-barrier model depending on the potential seen by an active electron removed from the target to the projectile ion or in the opposite direction. The projectiles are fully screened during the sub-sequent electron capture and loss.

2.1. Ion motion

As for the peripheral ion-cluster collision, trajectories are determined by using the Coulomb potential between projectiles and target clusters. In addition, projectiles can also be affected by the 'image charge' of charge $q' = -qa/R$ at a distance $R' = a^2/R$ from the center of the cluster. In order to conserve the total charge, a positive charge $-q'$ is placed at the center. Therefore, the SHCI of charge q at a distance R from the cluster center is subject to three forces. That is

$$F(q,s,R) = \frac{(q-s)q}{R^2} + \frac{a(q-s)^2}{R^3} - \frac{a(q-s)^2R}{(R^2-a^2)^2}, \quad (1)$$

where s is the charge state of the cluster at a distance R from the cluster center. The first force is the Coulomb force between the projectile ion and the net charge of the cluster. The second force is the interaction between the projectile ion and the positive charge $-q'$ placed at the center of the cluster and the last force comes from the "image charge".

2.2. Potential barrier and ionization potential

As for a single active electron at a distance x from the center of an infinitely neutral conducting sphere, the electric field affecting the electron is

$$E(x) = -\frac{q'_{\rm e}}{x^2} + \frac{q'_{\rm e}}{x-x'}, \quad (2)$$

where $x' = a^2/x$ is the position of the active electron self-image, $q'_{\rm e} = q_{\rm e}/x$ is the electron image charge. We calculate the work required to move an electron to infinity

$$W_1 = -\int_x^\infty q_{\rm e}E(x)\,{\rm d}x = -\frac{1}{2}\left(\frac{a}{x^2} - \frac{a}{x^2-a^2}\right). \quad (3)$$

The potential out of the cluster consists of two terms, one monopole Coulomb potential from the projectile ion and one dipole made up of image charges. In addition, if an electron tries to leave the cluster sphere, an image charge induced by the electron should also be considered. Therefore, the potential seen by the electron as it leaves the target includes not only the monopole Coulomb potential of the projectile and the residual target ions, but also the image potential of the projectile and of the electron due to the conducting spherical surface. Then, we have

$$U_{\rm e}^s(x) = -\frac{q-s+1}{R-x} + \frac{a(q-s+1)}{Rx-a^2} - \frac{a(q-s+1)}{Rx} - \frac{s}{x} + \frac{1}{2}\left(\frac{a}{x^2} - \frac{a}{x^2-a^2}\right), \quad (4)$$

where x is the position of the electron related to the center of target, $s-1$ is the charge state of the cluster, q is the initial charge state of the projectile ion. This barrier approach was described as a unified method in Ref. [6].

The energy required to ionize the conducting sphere of charge $(s-1)$ is

$$I_s^* = I_s + \frac{q-s+1}{R}, \quad (5)$$

where I_s is the ionization potential of a metal cluster without an external electric field. The second term in I_s^* is the Stark-shift caused by the projectile ion, which raises the ionization potential.

Here we apply the metallic plasma model[29] to estimate the ionization potential ($V_{\rm i}$) of the isolated neutral metal cluster, which is

$$V_{\rm i} = W_\infty \left[\frac{2a}{2a+d} + \frac{4d^2+2ad}{(a-d)^2}\right], \tag{6}$$

where W_∞ is the work function of the bulk copper and d can be expressed by W_∞ as

$$d = \frac{{\rm e}^2}{16\pi\varepsilon_0 W_\infty}, \tag{7}$$

where ε_0 is the electric permittivity of the free space. Then, we assume that the ionization potential of the isolated metal cluster with charge s is

$$I_s = V_{\rm i} + (s-0.5)/a. \tag{8}$$

This formula has been used in Ref. [30] to calculate the ionization potential of a metal sphere. The procedure can be physically motivated by noting that the ionization potential can be described as the sum of short-range pieces with sizes near the work function of metal copper, and a long-range piece due to the energy required to move the electron to infinity from the residual charged metal sphere.

2.3. The charge-exchange processes

According to the over-barrier model, as a projectile ion approaches a target, the electrons in the target can be resonantly captured by the projectile ion if the potential barrier $V_{\rm B}^s = U_{\rm e}^s({\rm max})$ ($U_{\rm e}^s({\rm max})$ is the maximum of potential $V_{\rm B}^s(x)$) is smaller than the ionization potential of the target. A series of electron resonant captures will happen during the collision. Assuming that the projectile ion is fully screened by the transferred electrons from the metal cluster, the charge evolution of the system obeys the following equation:

$$q_p(t) + q_c(t) = q_0 + N_{\rm AI}(t) = q, \tag{9}$$

where $N_{\rm AI}$ is the total number of Auger electrons emitted before time t, q_0 is the initial charge of a projectile ion.

With the approach of the projectile ion to the metal cluster and the transfer of electrons to the ion, the ionization potential and potential barrier will be rearranged. When a number of electrons are captured by a projectile, the energy level of an outer shell electron will rise because of the screening of the inner shell electron and the effect of the image charge. If the energy level lies above its ionization potential, the electrons in the projectile ion will be lost into the cluster resonantly. The Cowan code[31] is adopted to estimate the fast intra-atomic Auger transition rate for $n > 3$ in vacuum

$$A_{n,n'} = \frac{5.06\times10^{-3}}{|\Delta n|^{3.46}}, \tag{10}$$

where $\Delta n = n - n'$ is the smallest allowed quantum jump between the initial shell n with two active electrons and the final shell n' with bound electrons. The inner-shell (K–, L–, and M–shell) Auger transitions rates given in Refs. [32] and [33] are used.

Recombination of inner shell vacancies accompanied by the emission of fast Auger electrons or soft X-rays mainly takes place in the projectile hollow ion relaxation cascade.[34] We followed U. Thumm's work to describe the dynamics of projectile ion occupations, including the resonant multi-electron capture from the metal cluster, resonant loss, and intra-atomic Auger de-excitation. The population p_n of the $n_{\rm th}$ shell can be described by the following equation:

$$\begin{aligned}\frac{{\rm d}}{{\rm d}t}p_n =\ & \Theta(s_n - p_n)\Gamma_{\rm RC} - p_n\Gamma_{\rm RL} \\ & + \omega_n^{\rm fin}\sum_{n'>n} A_{n',n}\omega_{n'}^{\rm ini} \\ & - 2\omega_n^{\rm ini}\sum_{n'<n} A_{n,n'}\omega_{n'}^{\rm fin},\end{aligned} \tag{11}$$

where $\Gamma_{\rm RC}$ and $\Gamma_{\rm RL}$ are the resonant capture (RC) rate and resonant loss (RL) rate, respectively. $A_{n,n'}$ is the projectile fast Auger ionization rate. $\omega_n^{\rm fin}$, approximately equal to $(1+1.5p_n)^{-1}$, is an empirical reduction factor of the Auger decay due to partial population of the final n-shell population.[17] $\omega_n^{\rm ini}$ equals $0.5(p_n-1)p_n\Theta(p_n-2)$, which is the enhancement factor of Auger decay due to the multiple occupation of the initial shell. By integrating the rate Eq. (11), we can obtain the occupation number at any time. Our simulation did not include slow Auger transitions, because it took a much relaxation longer time than fast Auger transitions needed. This has been discussed in Ref. [22], where the relaxation time needed for the projectile ion is about 600 fs or 10^4 a.u. after the closest approach, which goes far beyond our simulation range.

The resonant capture state can be estimated by the energy conservation equation, which means that the binding energy of the $s_{\rm th}$ active electron localized to the target is equal to the resonant binding energy for the same electron localized to the projectile. Thus, we can obtain

$$\begin{aligned}E_{\rm B}^s =\ & \frac{q-2s+1}{R_s} + \frac{a(q-s+0.5)}{R_s^2-a^2} \\ & - \frac{a(q-s+0.5)}{R_s^2} + I_s,\end{aligned} \tag{12}$$

where R_s is the distance between the projectile ion and target. Therefore, the quantum number of the state in which the $s_{\rm th}$ electron fills is $n^s = q\sqrt{1/2E^s_{\rm B}}$.

2.3.1. RC rate

We have extended the classical approximations of electron capture rate in Ref. [17]. The capture rate is written in terms of the geometric cross section of the "saddle" on cluster and the current density of electrons as

$$\Gamma^s_{\rm RC} = \sigma(t) j^s_{\rm RC}(t), \tag{13}$$

where $j^s_{\rm RC}(t)$, the flux of electrons escaping from the cluster, is simply given in the Fermi gas approximation, with the density of states per unit volume, $g(\epsilon) = \sqrt{a\epsilon}/\pi^2$, by

$$j^s_{\rm RC}(t) = \frac{1}{4}\int_{V_{\rm B}}^{E_{\rm e}} g\epsilon\sqrt{2\epsilon}{\rm d}\epsilon, \tag{14}$$

where the lower limit of this integral is the potential energy. The upper limit is the least bound electron energy calculated with the charge of projectile ion and the cluster at time t. Here, we employ the expression of the geometrical cross section of the saddle for the electron transition[22] as

$$\sigma_{\rm B} = \begin{cases} \pi x^2_{\rm B} & I^*_s > V_{\rm B}, \\ 0 & I^*_s \le V_{\rm B}, \end{cases} \tag{15}$$

where the width $x_{\rm B}$ of the classically allowed transition region in the projectile-target direction can be calculated simply by $U_{\rm e}(x_{\rm B}) = I^*_x$.

2.3.2. RL rate

An electron can also be lost when its energy level reaches or exceeds the potential barrier. The resonant loss rate is decided by the frequency of the electron colliding with the potential wall and the probability of the electron hitting the 'saddle', that is

$$\Gamma^n_{\rm RL}(R) = \Theta(p_n - 1)P(R, \epsilon_n)\nu_n(R), \tag{16}$$

where $\nu_n(R)$, the frequency of projectile electrons in level n colliding with the potential wall, is approximately given by the revolution frequency in a Coulomb orbit

$$\nu_n(R) \simeq \frac{q^2_n(R)}{2\pi n^3}. \tag{17}$$

The probability[22] of an active electron hitting the saddle is estimated as

$$P(R, \epsilon_n) = \begin{cases} 1 & (\sigma_{\rm B} > \sigma_n), \\ \sigma_{\rm B}/\sigma_n & (\sigma_{\rm B} \le \sigma_n), \end{cases} \tag{18}$$

where σ_n is the overlapped area between a sphere of radius $\langle r_n\rangle$ and a plane which is through $R_{\rm B}$ and perpendicular to the "projectile-target axis". $R_{\rm B}$ is the distance where the resonant-loss condition is just satisfied under the same charge state. $\langle r_n\rangle$ is the radius of projectile electrons in level n, defined as the average of the overall orbital angular momentum

$$\langle r_n\rangle = \frac{5n^2+1}{4q_nR}. \tag{19}$$

The radius of the area σ_n is

$$x_n(R) = \sqrt{\langle r_n\rangle^2 - (R - R^2_{\rm B})}. \tag{20}$$

Such that the area is $\sigma_n = \pi x^2_n(R)$.

2.4. X-ray emission

The X-ray spectrum is very important for us to study the inner-shell charge exchanging its clock property,[35] involving the matching of the energy of X-ray lines and the electron distribution of the projectile ion while de-exciting. When the slow highly charged ion Ar^{q+} interacts with the metal cluster, a hollow ion is formed in the approaching process. The M and higher shells are mainly filled by resonant capture. The L shell is slowly fed mainly via Auger transitions. The KL^x lines, which are observed during the filling of a K hole, can be used to test and verify the electron occupation state in experiments. In our simulation, we employed the transition rates (both Auger and the X-ray decay) of M, L, and K shells proposed by Winecki *et al.*[32] The transition rates are expressed as a function of shell populations, and the decay rates of K_α and K_β can be obtained by $\Gamma = 3.04\times10^{-4}(2-n_{\rm K})n_{\rm L}\Theta(n_{\rm L}-1)$ and $\Gamma = 2.49\times10^{-5}(2-n_{\rm K})n_{\rm M}\Theta(n_{\rm M}-1)$, where $n_{\rm K}$, $n_{\rm L}$, and $n_{\rm M}$ are the electron number of K, L, and M shells, and $\Theta(n_n-1)$ is the step function. The energy of KL^x lines is calculated by formulas[32,36–38]

$$\begin{aligned} E_{\rm K\alpha} &= 3144.3 - 22.2n_{\rm L} - 4.9n_{\rm M} + 0.4n_{\rm L}n_{\rm M}, \\ E_{\rm K\beta} &= 3702.4 - 60.7n_{\rm L} - 15.9n_{\rm M} + 1.5n_{\rm L}n_{\rm M}. \end{aligned} \tag{21}$$

3. Results and discussion

In our simulation, the Mackey icosahedron structure copper cluster Cu_n ($n = 147, 309$) simulated results applying the EAM model by using Monte Carlo method in Ref. [27] are used because of its higher sym-

metry and stability. Details are presented in Fig. 1.

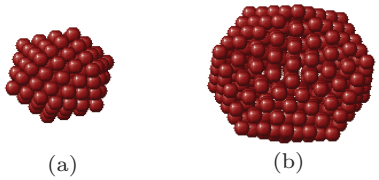


Fig. 1. (colour online) The structures of (a) Cu_{147} and (b) Cu_{309}.

3.1. The evolution of charge states, occupations and electron emissions

Figure 2 shows the evolution of a projectile and the target charge state, and the total number of Auger electrons emitted during the collision of 80 keV Ar^{17+} ions with Cu_{147} and Cu_{309} with an impact parameter $b = 15$ and $b = 25$ a.u.. The distance $R_{||}$ is the projection of the target–projectile distance onto the incident-beam direction. The closest point is given when $R_{||} = 0$. From this figure, we find that the charge exchange mainly occurs on the incident trajectory ($R_{||} < 0$), starting at $R_{||} = -30.6$ and $R_{||} = -41.0$, respectively, which corresponds to the first critical over-barrier distance $R^* = 34.1$ and $R^* = 48.0$. Subsequently, the projectile ion captures additional electrons and reaches the lowest charge state near the closest point. In Fig. 2(a), we find that it is possible to transfer about 10 electrons from a Cu_{147} target before reaching the closest point. Thereafter, resonant charge exchange stops and the target charge remains unchanged; the projectile charge increases slightly due to later Auger de-excitation. When the target comes to Cu_{309} in Fig. 2(b), the charge transfer is enhanced. The final charge state of a target cluster becomes higher compared to the smaller target cluster and rises up to 14. These phenomena are very similar to Thumm's results.[16,22] We find that the final charge state of the projectile ion is much larger than the cases in grazing incidence collisions with a metal surface. In our previous work,[36] the fraction of Ar^0, Ar^{1+} prevail over all about 93% under a much smaller incident angle. The difference may be mainly due to the short-range interaction of projectile ions with the target and the comparatively long interaction time. In the latter case, projectile ions can travel in electron gas on the metal surface for a long time and even collide with surface atoms, which leads to some other charge exchange mechanisms, such as side-feeding and peeling-off. In addition, in a grazing incident case, a relatively close collision leads to the rapid direct filling of inner shells. These differences can also be spotted in the population evolution of projectile ions and X-ray spectra (see subsequent discussions).

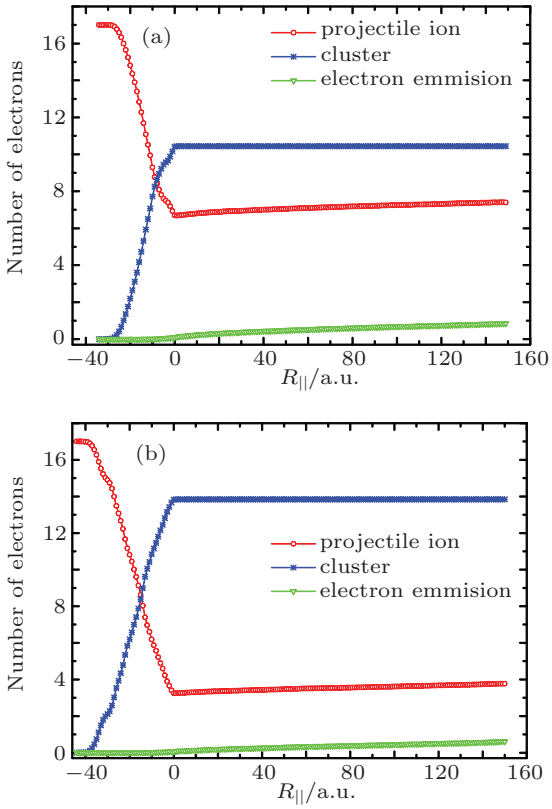


Fig. 2. (colour online) The charge-state evolution and the Auger emission for 80 keV(corresponding speed is $v = 0.28$) Ar^{17+} ions colliding with the copper cluster. (a) Collision with Cu_{147} with an impact parameter $b = 15$. (b) Collision with Cu_{309} with an impact parameter $b = 25$. $R_{||}$ is the projection distance of the target-projectile distance onto the incident-beam direction; at the closest approach $R_{||} = 0$.

Figure 3 gives more detailed dynamical information of the electronic transition, in which the evolution of projectile ion level occupations (instantaneous occupation minus the initial occupation) is showed. The impact parameters are the same as that in Fig. 2. According to Fig. 3(a), the electrons are firstly resonantly captured into projectile shells with the principal quantum number around $n = 12$. As the projectile further approaches the target cluster, relatively inner shells are more likely to be occupied and the occupation reaches the maximum around $n = 4$. It covers a large range of shells, but the arrangement of population changes rapidly before the closest point, and after that it changes slowly and the outer shells' electrons transfer slightly into inner shells, especially highly populated shells, by fast Auger transition. For the larger target case, as shown in Fig. 3(b), the highest resonantly populated shell rises up to $n = 16$. The most probable lower shells occupation is around

n = 3–5. These indicate that more shells will be occupied with the increase of the atom number of the target cluster.

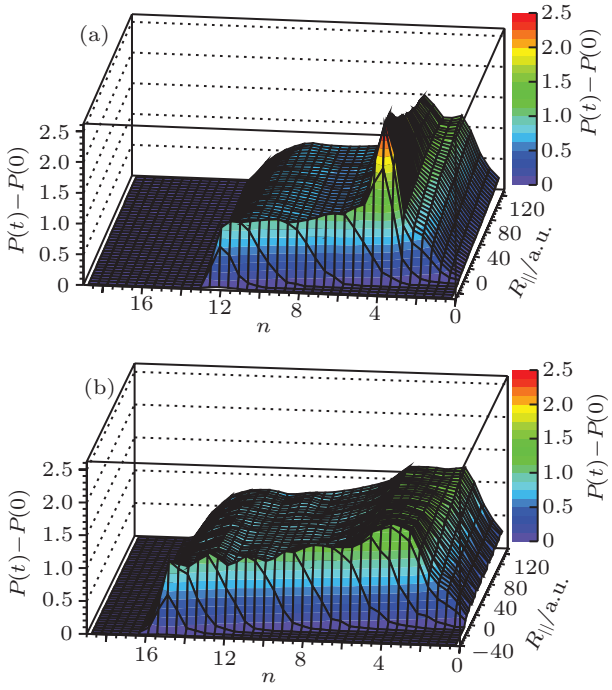


Fig. 3. (colour online) The evolution of the projectile ion level occupation changes with respect to the initial occupations. The occupation changes of projectile levels n (mainly the quantum number) as a function of $R_{||}$. (a) Collision with Cu_{147} with an impact parameter b = 15. (b) Collision with Cu_{309} with an impact parameter b = 25.

3.2. Impact-parameter dependence of charge states, occupations and electron emission

As shown in Fig. 4, the dependence of the final charge state($R_{||}$ = 150) of projectile ions and the corresponding targets with impact parameters are calculated. The value of the final charge state of projectile ions is between about 7.4 and 17.0 in Fig. 4(a) and ranges from 3.8 to 17.0 in Fig. 4(b). In a large impact parameter collision, the long range electrons captured from metal cluster by SHCIs can produce multiply charged clusters. The charge state of the cluster can be selected by operating the impact parameter. If we decrease the impact parameter, a cluster with a higher charge state could be produced. In fact, there is a critical impact parameter. Although the parameter is larger than the radius of the cluster, the cluster will also be destroyed. In our simulation, we set the limit as 14 a.u. for Cu_{147} and 24 a.u. for Cu_{309}. By assuming minimal impact parameters for the non-destructive collisions of b = 15 and b = 25, the highest final target charge states are predicted as 10.4 and 13.8 correspondingly. According to the simulation results, the Auger electron intensity decreases as the impact parameter becomes larger. For distant collisions ($b > 26$ for Cu_{147} and $b > 38$ for Cu_{309}), charge exchange still occurs, however, no Auger electron emission is observed. This is because at least two electrons are required in a shell for the fast Auger transition. However, the final average electron number in each shell is no more than 0.8 in the cases where $b > 26$ and $b > 38$ respectively for both Ar^{17+}–Cu_{147} and Ar^{17+}–Cu_{309} collisions.

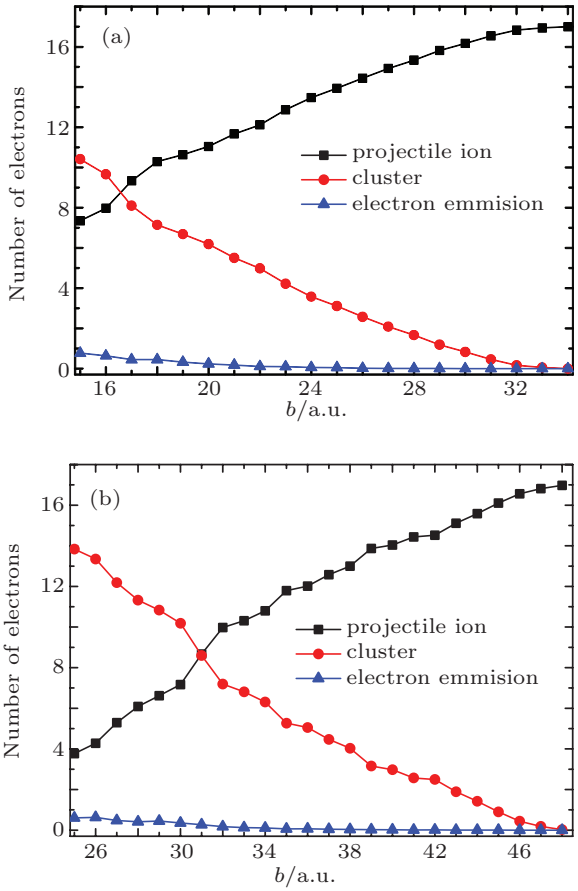


Fig. 4. (colour online) The final charge state and the emitted Auger electron number for 80 keV Ar^{17+} ions colliding with copper clusters as a function of the impact parameter. (a) Collision with a Cu_{147} target. (b) Collision with a Cu_{309} target.

Figure 5 shows that the final occupation of the projectile at a distance $R_{||}$ = 150 changes with the impact parameters. We find that no more than half of the electrons fills in the high levels in large impact parameters $b > 29$ (a) and $b > 44$ (b) cases. This is because the critical distances at which the first resonant electron transition occurs are about R_1^* = 34.1 and 48.0 respectively, and the resonant capture rate related to the time that a projectile intersects with a sphere of radius R_1^* around the cluster. A larger impact parameter leads to lower electron transition. In

addition, captured electrons in the high levels may be also lost because of the changing of the potential barrier. With the decrease of b, captured electrons subsequently tend to be distributed in lower shells and the number of electrons filling each shell increases correspondingly. Thus, the fast Auger electron yield will also increase, which will accelerate lower shell filling. If we pay attention to the lower shells, we note that number of electrons in these shells increases dramatically as the parameter becomes smaller. There is a peak of population occupation around $n = 5$ at $b = 15$ in Fig. 5(a). However, this peak shifts towards lower shells around $n = 3$ at $b = 25$ and is extended in Fig. 5(b). Combining with Fig. 3, it is easy to suppose that the X-ray intensity of the latter will be stronger than the former.

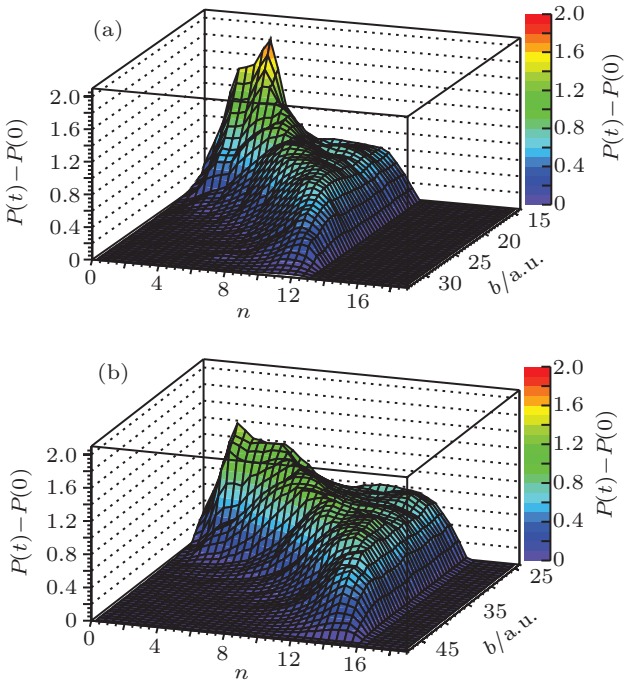


Fig. 5. (colour online) The final occupation changes of the projectile level n for 80 keV Ar^{17+} ions colliding with (a) Cu_{147} and (b) Cu_{309} clusters as a function of the impact parameter.

3.3. X-ray emission, Auger spectra and scattering angle

The K-shell vacancy decay of SHCI Ar^{17+} interacting with a metallic cluster at a large impact parameter can also be studied by investigating the K X-ray spectrum. Figure 6 is the Kα X-ray spectrum of Ar^{17+} during the peripheral colliding with Cu_{147} and Cu_{309} clusters at the impact parameters $b = 15$ and $b = 25$, respectively. The intensities presented in the figures are normalized. The absolute intensity of the Kα X-ray of the latter is twice that of the former. In Fig. 6(a), We can easily observe that there are only 3 peaks. The intensity of the KL^1 line is the strongest one among these satellite lines, the intensity of the KL^2 line is only 1/8 that of the KL^1, and the intensity of the KL^3 line is the smallest. From the Kα X-ray spectrum of the Ar^{17+} colliding with a larger cluster target, shown in Fig. 6(b), we note that the intensities of KL^2 and KL^3 lines are enhanced compared with the ones in Fig. 6(a). In our simulation, other KL^x (x = 4–8) lines are hardly observed. The relative intensity of the KL^x lines depends only on the rate at which the L shell is filled compared to the filling rate of the K vacancies. The L shell filling rate is related to the initial

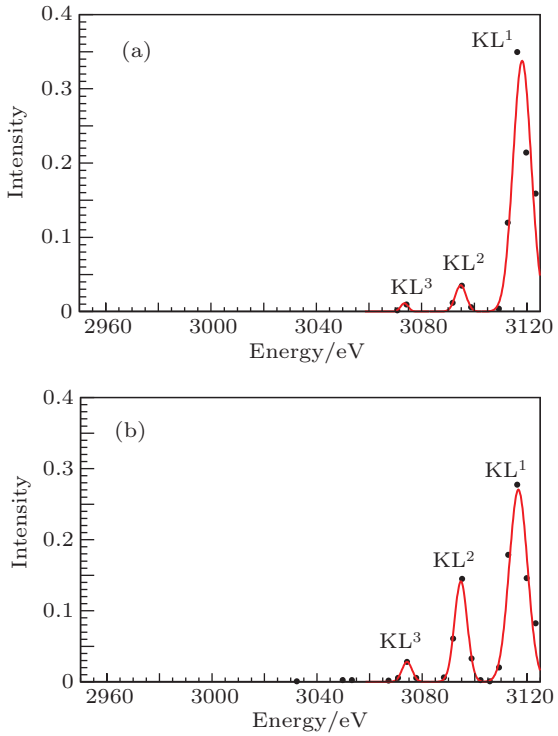


Fig. 6. (colour online) The Kα X-ray spectrum observed with Ar^{17+} ions. (a) Collision with Cu_{147} clusters under $b = 15$. (b) Collision with Cu_{309} clusters under $b = 25$. Impact energy is 80 keV. The solid lines are guidelines.

state that the electrons have been captured in and the initial number of captured electrons. The main mechanisms that contribute to the filling of L-shell vacancies are Auger transition and radiative decay. Within our simulation, Lα X-rays only contribute a very minor part to the L shell filling, which is consistent with Ref. [32]. Therefore, the main way of filling a L shell is fast Auger transition. However, it is not sufficient to transmit enough electrons into the inner shell, which can also be found in Fig. 3, where the maximum of the average occupation is no more than 3 in a $n = 2$ shell under the same incidence conditions. That is

why only 3 peaks can be observed in the Kα X-ray spectra.

The spectrum of emitted Auger electrons in 100 eV wide energy bins by the time when the projectile reaches the distance $R_{||} = 150$ is displayed in Fig. 7. Through calculation, we know that the energy ranges of KLL, KLM, KMM, and LMM Auger electrons are about 2300–2500 eV, 2800–3000 eV, 3400–3500 eV, and 100–400 eV, respectively. It can be seen that the relative intensities the Auger electron emission of these inner shells, shown in Fig. 7(b), are enhanced compared with those in Fig. 7(a). This demonstrates that electrons fill inner shells more easily before projectile ions reach the closest points on their coming traces and most Auger electron emission occurs on the leaving traces.

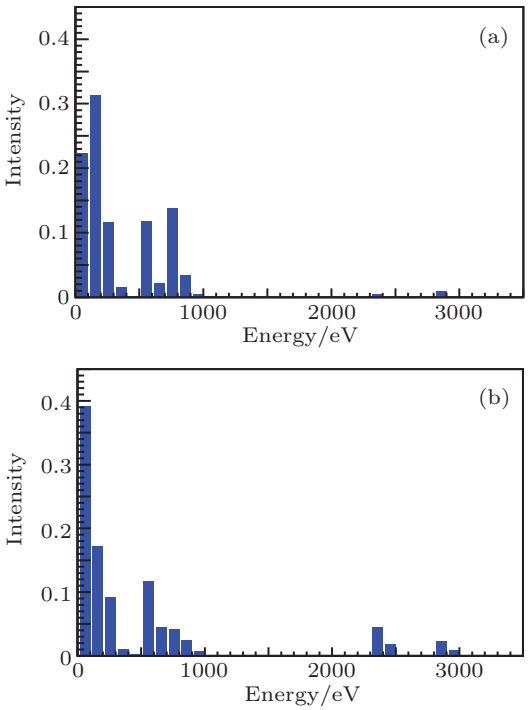


Fig. 7. (colour online) The Auger-electron spectra, normalized, integrated over energy, and binned in 100 eV. (a) Collision with Cu_{147} clusters under $b = 15$. (b) Collision with Cu_{309} clusters under $b = 25$. Impacting energy is 80 keV.

The projectile angular scattering distribution is obtained by integrating the transversal momentum transfer to the projectile along many random selected trajectories and we find that the distribution curves are similar with parabolas (Fig. 8). In Fig. 8(a), the scattering angle becomes larger with the increase of the final charge of the cluster, and reaches its maximum at about 0.1027°) when the charge equals 12. Thereafter, it declines to 0.0891°) when the charge equals 15. In a similar way, it reaches its maximum at about 0.0218°) when the charge is 11 (Fig. 8(b)). This is mainly due to the interaction of projectile ions with the "image charge" on the clusters, which also demonstrates the existence of the critical impact parameter under which the incident ions will collide directly with targets.

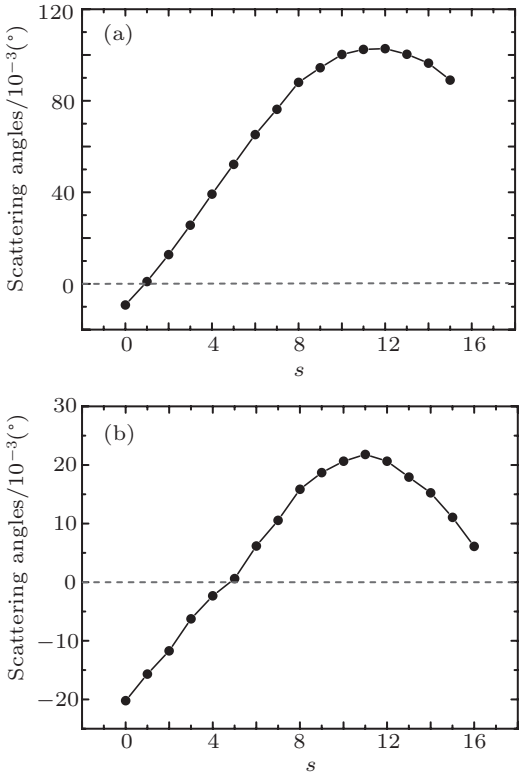


Fig. 8. The most likely scattering angles θ as a function of the charge of the cluster s. (a) Collision with Cu_{147}. (b) Collision with Cu_{309}.

4. Conclusion

In this work we investigated the interaction of highly charged ions colliding with large spherical metal clusters at large impact parameters. The ions' motion and charge-exchange processes are described on the basis of the dynamic classical over-barrier model. In our simulation, we follow the trail of projectile ions and observe the formation of hollow ions during the interaction of highly charged Ar^{17+} ions with different copper clusters. We have found that the charge-exchange happens at a critical distance between the HCI and the cluster, with the decreasing of which the charge state of the cluster reaches the top at the closest point around $R_{||} = 0$. After that the resonant charge-exchange stops and the projectile relaxes mainly through Auger electron and X-ray emission. With the increasing of the impact parameter, fewer electrons will be transferred during the collision. The evolution of the population occupation of

projectile ions and the relationship of the final occupation with different impact parameters are presented. The results show that the closer the impact is, the more electrons will fill the inner shells. This is also strongly confirmed by the X-ray and Auger electron emission. The K-shell vacancy decay during the interaction of Ar^{17+} with metallic clusters at large parameter incidence is also observed by investigating the K X-ray spectra, from which we have found that the inner shells can hardly be filled by direct electron transfer, and is mainly through Auger processes instead. Furthermore, under the same ratio between the impact parameter and the radium of the cluster, the charge transfer, X-ray and Auger electron emission are all enhanced. In addition, we predict the scattering angle θ as a function of the charge state of the cluster, and the curves are similar to parabolas.

References

[1] Cederquist H, Fardi A, Haghighat K, Langereis A, Schmidt H T and Schwartz S H 1999 *Phys. Scr.* **T80** 46

[2] Niehaus A 1986 *J. Phys.* B: *At. Mol. Phys.* **19** 2925

[3] Heer W A 1993 *Rev. Mod. Phys.* **65** 611

[4] Walch B, Cocke C L, Voelpel R and Salzborn E 1994 *Phys. Rev. Lett.* **72** 1439

[5] Bárány A and Setterlind C J 1995 *Nucl. Instrum. Methods Phys. Res.* B **98** 184

[6] Briand J P, d'Etat-Ban B, Schneider D, Briere M A, Decaux V, McDonald J W and Bardin S 1996 *Phys. Rev.* A **53** 2194

[7] LeBrun T, Berry H G, Cheng S, Dunford R W, Esbensen H, Gemmell D S, Kanter E P and Bauer W 1994 *Phys. Rev. Lett.* **72** 3965

[8] Biquard X, Guet C, Huber B, Jalabert D, Maurel M, Opitz J and Rocco J C 1997 *Phys. Scr.* **1997** 291

[9] Itoh A, Tsuchida H, Miyabe K, Imai M and Imanishi N 1997 *Phys. Scr.* **1997** 289

[10] Langereis A, Jensen J, Fardi A, Haghighat K, Schmidt H T, Schwartz S H, Zettergren H and Cederquist H 2001 *Phys. Rev.* A **63** 062725

[11] Schwartz S H, Fardi A, Haghighat K, Langereis A, Schmidt H T and Cederquist H 2000 *Phys. Rev.* A **63** 013201

[12] Cederquist H, Fardi A, Haghighat K, Langereis A, Schmidt H T, Schwartz S H, Levin J C, Sellin I A, Lebius H, Huber B, Larsson M O and Hvelplund P 2000 *Phys. Rev.* A **61** 022712

[13] Wang L, Zhang X A, Yang Z H, Chen X M, Zhang H Q, Cui Y, Shao J X and Xu X 2008 *Acta Phys. Sin.* **57** 0137 (in Chinese)

[14] Daligault J, Chandezon F, Guet C, Huber B A and Tomita S 2002 *Phys. Rev.* A **66** 033205

[15] Ryufuku H, Sasaki K and Watanabe T 1980 *Phys. Rev.* A **21** 745

[16] Thumm U 1997 *Phys. Rev.* A **55** 479

[17] Burgdörfer J and Lerner P and Meyer F W 1991 *Phys. Rev.* A **44** 5674

[18] Guillemot L, Roncin P, Gaboriaud M N, Laurent H and Barat M 1990 *J. Phys.* B: *At. Mol. Opt. Phys.* **23** 4293

[19] Ducrée J J, Casali F and Thumm U 1998 *Phys. Rev.* A **57** 338

[20] Jin Jian, Khemliche H, Prior M H and Xie Z 1996 *Phys. Rev.* A **53** 615

[21] Brenac A, Chandezon F, Lebius H, Pesnelle A, Tomita S and Huber B A 1999 *Phys. Scr.* **1999** 195

[22] Thumm U 1994 *J. Phys.* B: *At. Mol. Opt. Phys.* **27** 3515

[23] Thumm U, Bárány A, Cederquist H, Hägg L and Setterlind C J 1997 *Phys. Rev.* A **56** 4799

[24] Selberg N, Bárány A, Biedermann C, Setterlind C J, Cederquist H, Langereis A, Larsson M O, Wännström A and Hvelplund P 1996 *Phys. Rev.* A **53** 874

[25] Plagne L and Guet C 1999 *Phys. Rev.* A **59** 4461

[26] Groß M and Guet C 1996 *Phys. Rev.* A **54** R2547

[27] Pan X D, Gai Z G and Li G P 2008 *Chin. Phys.* B **17** 3329

[28] Jackson J D 1975 *Classical Electrodynamics* (New York: Wiley)

[29] Halas S 2006 *Materials Science Poland* **24** 4

[30] Zettergren H, Schmidt H T, Cederquist H, Jensen J, Tomita S, Hvelplund P, Lebius H and Huber B A 2002 *Phys. Rev.* A **66** 032710

[31] Cowan R D 1981 *The Theory of Atomic Structure and Spectra* (Berkeley: University of California Press)

[32] Winecki S, Cocke C L, Fry D and Stöckli M P 1996 *Phys. Rev.* A **53** 4228

[33] Bhalla C P 1973 *Phys. Rev.* A **8** 2877

[34] Winter H and Aumayr F 1999 *J. Phys.* B: *At. Mol. Opt. Phys.* **32** R39

[35] d'Etat B, Briand J P, Ban G, de Billy L, Desclaux J P and Briand P 1993 *Phys. Rev.* A **48** 1098

[36] Luo X W, Hu B T, Zhang C J, Wang J J and Chen C H 2010 *Phys. Rev.* A **81** 052902

[37] Wang J J, Zhang J, Gu J G, Luo X W and Hu B T 2009 *Phys. Rev.* A **80** 062902

[38] Zou X R, Shao J X, Chen X M and Cui Y 2010 *Acta Phys. Sin.* **59** 6064 (in Chinese)